Journal of Sound and Vibration (1995) **184**(1), 35–58

ANALYSIS OF PERIODICALLY EXCITED NON-LINEAR SYSTEMS BY A PARAMETRIC CONTINUATION TECHNIQUE

C. Padmanabhan and R. Singh

Acoustics and Dynamics Laboratory, *Department of Mechanical Engineering*,
The Ohio State University, 206 *West* 18*th Avenue*, *Columbus Ohio* 43210-1107, *U.S.A.*

(*Received* 22 *September* 1993, *and in final form* 11 *April* 1994)

The dynamic behavior and frequency response of harmonically excited piecewise linear and/or non-linear systems has been the subject of several recent investigations. Most of the prior studies employed harmonic balance or Galerkin schemes, piecewise linear techniques, analog simulation and/or direct numerical integration (digital simulation). Such techniques are somewhat limited in their ability to predict all of the dynamic characteristics, including bifurcations leading to the occurrence of unstable, subharmonic, quasi-periodic and/or chaotic solutions. To overcome this problem, a parametric continuation scheme, based on the shooting method, is applied specifically to a periodically excited piecewise linear/non-linear system, in order to improve understanding as well as to obtain the complete dynamic response. Parameter regions exhibiting bifurcations to harmonic, subharmonic or quasi-periodic solutions are obtained quite efficiently and systematically. Unlike other techniques, the proposed scheme can follow period-doubling bifurcations, and with some modifications obtain stable quasi-periodic solutions and their bifurcations. This knowledge is essential in establishing conditions for the occurrence of chaotic oscillations in any non-linear system. The method is first validated through the Duffing oscillator example, the solutions to which are also obtained by conventional one-term harmonic balance and perturbation methods. The second example deals with a clearance non-linearity problem for both harmonic and periodic excitations. Predictions from the proposed scheme match well with available analog simulation data as well as with multi-term harmonic balance results. Potential savings in computational time over direct numerical integration is demonstrated for some of the example cases. Also, this work has filled in some of the solution regimes for an impact pair, which were missed previously in the literature. Finally, one main limitation associated with the proposed procedure is discussed.

1. INTRODUCTION

Piecewise linear or non-linear characteristics including clearances are found in many machine elements and assemblies, such as gears, bearings, clutches, etc. Such non-linear systems are often excited periodically while under the influence of a mean force or torque. The knowledge of steady state solutions, such as the frequency response characteristics, is essential from a dynamic design as well as a noise and vibration control viewpoint. Typical investigations have used one of the following solution techniques: (a) piecewise-linear techniques [1, 2], (b) harmonic balance methods [3–7], (c) analog simulation methods [8, 9] and (d) direct time-domain numerical integration [9–12]. Since non-linear systems, exhibit phenomena such as multiple solution regimes, subharmonic, and quasi-periodic and chaotic solutions, it is desirable to locate parameter regions in which such solutions occur in an efficient and unambiguous manner, which is the focus of this paper. Such an analysis, for instance by using direct numerical integration, can only be accomplished by

0022–460X/95/260035 + 24 $12.00/0

sweeping large initial condition maps. This procedure is obviously a rather laborious process, especially when the dimension of the problem increases. The harmonic balance schemes, which are usually variants of the Galerkin method [13], are also limited in their ability to track parameter bifurcations leading to the complex phenomena described earlier, although a few attempts have been made towards that goal [3–6]. For instance, Comparin and Singh [7] could not explain some of the analog simulation results using their describing function approximation [14].

Alternatively, computational techniques such as the shooting method [15–18] have been used to locate the fixed points of Poincaré maps (and hence the periodic solutions) and to determine their stability, as well as to obtain resonance backbone curves and other dynamic characteristics very efficiently. Ling [15] has tested the shooting method for a variety of single- and two-degree-of-freedom non-linear systems, usually with cubic non-linearities, and found the technique to be extremely useful. Sato *et al*. [18] applied the technique to map the tangent and pitchfork bifurcations in a gear pair with backlash and a periodic time-varying gear mesh-stiffness. The conventional shooting methods can be used to efficiently detect bifurcations, in conjunction with a parameter path following technique [19–21], but previous investigations have limited their application to autonomous systems. Such a technique has yet to be widely applied to the analysis of externally forced non-linear systems, especially those described earlier. Accordingly, the main objective of this paper, based on the literature reviewed above, is to adapt a parametric continuation (or path following) scheme, in conjunction with the shooting method, in order specifically to study the dynamics of periodically forced piecewise non-linear systems. The proposed continuation procedure is first validated by applying it to a Duffing oscillator, and the results are compared with those reported in the literature, as well as with predictions yielded by commonly used perturbation and one-term harmonic balance schemes. Then, the proposed scheme is used to re-investigate the impact pair problem of Comparin and Singh [7]. An attempt is made to fill in some of the subharmonic solutions and other regimes which were missed in their investigation. Both harmonic and periodic excitations are considered and the various solution regimes are mapped completely.

2. POINT MAPPING FOR PERIODIC SOLUTIONS

2.1. SIMPLE SHOOTING METHOD

The general governing equation for a periodically forced (with fundamental excitation frequency Ω) non-linear system with N degrees of freedom (DOF) can be written in state space form, of dimension $2N$, as follows (see Appendix A for the identification of symbols):

$$\mathbf{q}' = \mathbf{F}(\mathbf{q}; \Omega\tau), \tag{1}$$

where the state vector $\mathbf{q}$ is defined as

$$\mathbf{q} = [q_1 \quad \cdots \quad q_{2N}]^{\mathrm{T}}, \qquad q_{i+1} = q_i', \quad i = 1, 3, \ldots, 2N-1. \tag{2, 3}$$

Here the q_i's and q_{i+1}'s ($i = 1, 3, \ldots, 2N-1$) represent the displacements and velocities, respectively, of the non-linear system. The force vector $\mathbf{F}$ can be further divided into linear, non-linear and periodic excitation components, as

$$\mathbf{F} = \mathbf{A}\mathbf{q} + \mathbf{h}(\mathbf{q}) + \mathbf{T}(\boldsymbol{\Omega}\tau). \tag{4}$$

A number of investigators [15, 17–20] have used the shooting method which transforms an initial value problem into a two-point boundary value problem. Since we are interested in finding the periodic solutions, we need $q_i(0)$ such that $q_i(0) = q_i(m\tau_0)$; $\tau_0 = 2\pi/\Omega$, $i = 1, \ldots, 2N$, where m is a positive integer. For instance, $m = 1$ would solve for period-1

(P1) solutions, while $m = 2$ would solve for period-2 (P2) subharmonic solutions. Furthermore, the technique is capable of finding both stable as well as unstable periodic solutions. The simple shooting technique is now described below in detail.

Choose initial conditions, $q_i(0) = \eta_i$, $i = 1, \ldots, 2N$. An appropriate method for selecting these initial guesses is discussed in detail in section 2.1.1. The system of equations described by equations (1)–(4) can then be solved, say for $m = 1$, from $\tau = 0$ to $\tau = \tau_0$, by using any numerical integration scheme. *All subsequent equations are for* $m = 1$. We employ DOPRI5 [22], which is a fifth order Runge–Kutta scheme with step size control and uses an error estimator based on the fourth order Runge–Kutta formula. The values $q_i(\tau_0)$ depend on the choice of the initial conditions, η_i, and also implicitly on the value of a parameter, say α, as shown below:

$$q_i(\tau_0) = \Phi_i(\boldsymbol{\eta}; \alpha), \qquad i = 1, \ldots, 2N. \tag{5}$$

Here, α typically could represent any system design variable, such as spring stiffness and damping coefficient, or external variables, such as the amplitude and frequency of the periodic forcing function. The periodicity boundary condition requires that the following equation be satisfied:

$$G_i(\boldsymbol{\eta}; \alpha) = \Phi_i(\boldsymbol{\eta}; \alpha) - \eta_i = 0, \qquad i = 1, \ldots, 2N. \tag{6}$$

For a given α, equation (6) represents $2N$ non-linear algebraic equations in $2N$ unknowns. This can then be solved iteratively by using a Newton–Raphson technique ($\mathbf{J}\Delta\boldsymbol{\eta}^{k+1} = -\mathbf{G}(\boldsymbol{\eta}^k)$). However, this procedure requires the formation and computation of the $2N \times 2N$ Jacobian matrix, $\mathbf{J}$, the elements of which are given by the equation

$$J_{ij} = \frac{\partial G_i}{\partial \eta_j} = \left\{\frac{\partial \Phi_i}{\partial \eta_j} - \delta_{ij}\right\}, \qquad i, j = 1, \ldots, 2N, \quad \delta_{ij} = \begin{cases} 1, & i = j \\ 0, & i \neq j \end{cases}. \tag{7, 8}$$

There are other quasi-Newton schemes, such as Broyden's scheme [23] or Warner's algorithm [24], which do not need the Jacobian explicitly to solve for the η_i's. However, as will be shown later, there is still a need to calculate the Jacobian explicitly, in order to obtain the eigenvalues which determine the stability of the periodic solution. The other two schemes do not yield good approximations to the Jacobian even though they converge to the same η_i's. From equation (7), it is clear that the $\partial\Phi_i/\partial\eta_j$ terms are unknown, and they cannot be obtained directly just by integrating equation (1). In order to obtain their magnitudes, additional variables $\mu_{ij}, i, j = 1, \ldots, 2N$, representing the change in the trajectory with respect to the initial guesses, $\eta_j, j = 1, \ldots, 2N$, are defined, and the equations describing them are derived from an infinitesimal variation of the governing differential equations (see equation (1)):

$$\mu_{ij}(\tau) = \frac{\partial q_i(\tau)}{\partial \eta_j}, \qquad i, j = 1, \ldots, 2N, \tag{9}$$

$$\mu'_{ij}(\tau) = \frac{\partial}{\partial \tau}\left\{\frac{\partial q_i(\tau)}{\partial \eta_j}\right\} = \frac{\partial}{\partial \eta_j}\left\{\frac{\partial q_i(\tau)}{\partial \tau}\right\} = \sum_{k=1}^{2N} \frac{\partial F_i}{\partial q_k}\mu_{kj}, \tag{10}$$

where the $\partial F_i/\partial q_k$ $(i, k = 1, \ldots, 2N)$ terms are obtained by differentiating equation (4) with respect to the q_i's. The required Jacobian can now be evaluated as

$$J_{ij} = \frac{\partial G_i}{\partial \eta_j} = \frac{\partial \Phi_i}{\partial \eta_j} - \delta_{ij} = \mu_{ij}(\tau_0) - \delta_{ij}, \qquad i, j = 1, \ldots, 2N. \tag{11}$$

From equation (9) it is apparent that the initial conditions for $\mu_{ij}(\tau)$ are $\mu_{ij}(0) = \delta_{ij}$. Now we integrate the governing equations for some $\alpha = \alpha^*$, given by equation (1), along with

the variational equations, given by equation (10), by using appropriate initial conditions from $\tau = 0$ to $\tau = \tau_0$, and then we apply the Newton–Raphson procedure until convergence is achieved. This results in the following equation to be satisfied:

$$\boldsymbol{\eta}^0 = \boldsymbol{\Phi}(\boldsymbol{\eta}^0; \alpha^*). \tag{12}$$

The solution η_i^0 is then a *fixed point* of the iteration process described above, i.e., it represents the solution of the Poincaré mapping of the system. Such a fixed point solution could be stable or unstable [15–18], the determination of which is discussed later.

2.1.1. *Choice of initial conditions*

In order to start the shooting procedure, initial conditions of the state variables, q_i, $i = 1, \ldots, 2N$, have to be chosen. Three specific ways are described below to aid the future users; other choices are also possible.

(a) *Initial conditions based on a random guess*. This procedure leads to a fast convergence of Newton iterations, when the strength of the non-linearity is small or if one chooses a parameter region where the effects of the non-linearity are negligible. In the examples solved in subsequent sections, the fixed point calculation (parameter of interest Ω) is started at a high frequency value, where the system is almost linear, to ensure quick convergence of the shooting procedure.

(b) *Homotopy approach*. When the above-mentioned procedure fails to converge, which usually happens in parameter regions where the non-linear effects are dominant, a homotopy approach has to be adopted. Equation (4) is re-written as

$$\mathbf{F} = \mathbf{A}\mathbf{q} + \mathbf{T}(\boldsymbol{\Omega}\boldsymbol{\tau}) + \boldsymbol{\theta}\mathbf{h}(\mathbf{q}), \qquad \theta \in [0, 1]. \tag{13}$$

When θ is equal to zero, then equation (13) is linear, while if θ is one then we retrieve equation (4). Hence, one begins with $\theta = 0$, and then adopts the approach used in (a). Once the fixed point has been calculated, its value is used as a starting guess for the calculation of the fixed point value at $\Delta\theta$ (a small increment). This ensures fast convergence of the Newton iteration process. A repeated application of this procedure, in steps of $\Delta\theta$, would then lead us to the appropriate starting guesses for $\theta = 1$.

(c) *Multiple shooting*. In (a) and (b), the shooting procedure is carried out over the time interval $[0, \tau_0]$ in one single step. An alternative is to use the multiple shooting approach [21], in which the time interval $[0, \tau_0]$ is divided into several user defined sub-intervals. The shortening of the time interval increases the domain of attraction of the Newton–Raphson method, thus reducing the adverse effects of bad initial guesses. However, this leads to an increased computational effort as compared with the simple shooting approach, due to additional continuity enforcing equations at each sub-interval boundary.

2.1.2. *Stability of the point mapping*

The stability is determined by the eigenvalues of the linearized mapping $\boldsymbol{\Phi}$, computed at the fixed points $\boldsymbol{\eta}^0$, to yield the monodromy matrix, $\mathbf{B}$ [19, 21, 25]:

$$\mathbf{B} = \left[\frac{\partial \Phi_i}{\partial \eta_j}\right]_{\boldsymbol{\eta}^0} = [\mu_{ij}(\tau_0)] = \{\mathbf{J} + \mathbf{I}\}|_{\boldsymbol{\eta}^0}, \qquad i, j = 1, \ldots, 2N. \tag{14}$$

The periodic solution is stable if the magnitude of the eigenvalues, $|\lambda_i|$ ($i = 1, \ldots, 2N$), is less than unity. The stability of the periodic solution changes when some λ_i crosses the unit circle. There are three different types of instabilities, as seen in Figure 1 (see, e.g., references [19, 21, 25] for more details): (i) $\lambda_i = -1$, period-doubling or *flip* bifurcation occurs; (ii) $\lambda_i = 1$, saddle-node or symmetry breaking bifurcation occurs; (iii) a pair of

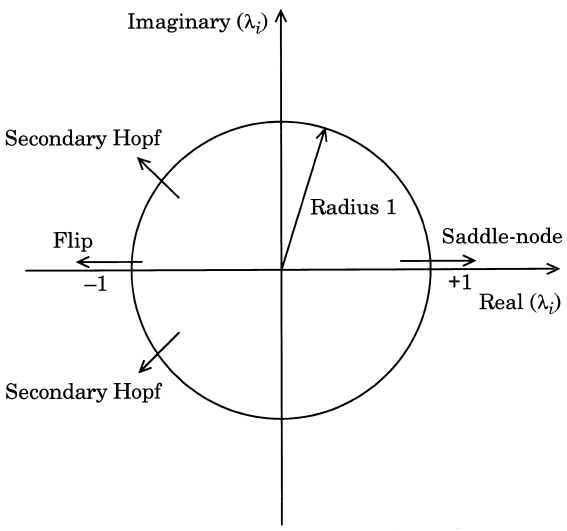

Figure 1. Modes of instability of a Poincaré map, $\lambda = +1$ saddle-node or symmetry breaking, $\lambda = -1$ flip or period-doubling and $|\lambda| = 1$ secondary Hopf instability.

complex conjugates ($|\lambda| = 1$) crosses the unit circle—this is termed as the secondary Hopf bifurcation.

2.2. A PATH FOLLOWING TECHNIQUE WITH THE SHOOTING METHOD

Often, one would like to know how the fixed points or the periodic solutions change as the parameter of interest is varied from α^*, for which the solution has already been determined, as outlined in section 2.1. A recursive application of the shooting method would be the easiest way to carry out such a task. One expects that $\boldsymbol{\eta}^0 = \boldsymbol{\Phi}(\boldsymbol{\eta}^0; \alpha^*)$ would be a good initial guess for $\boldsymbol{\eta}(\alpha^* + \Delta\alpha)$, to be used in the Newton–Raphson scheme, for a small increment $\Delta\alpha$. Once the iterations have converged we obtain the solution for $\alpha^* + \Delta\alpha$. In this manner, a branch of solutions over a range of the parameter α can be obtained. One of the drawbacks of such an approach is the lack of information about the continuity of the solution branch, as α is varied from α^* in increments of $\Delta\alpha$. For this purpose, the trajectory of the solution branch in the neighbourhood of α^* can be obtained from equation (6) by a Taylor series expansion (truncated to the first term) in α:

$$\sum_{k=1}^{2N} \left\{ \frac{\partial \Phi_i}{\partial \eta_k} - \delta_{ik} \right\} \frac{\partial \eta_k}{\partial \alpha} + \frac{\partial G_i}{\partial \alpha} = 0, \qquad i = 1, \ldots, 2N. \tag{15}$$

Equation (15) represents a linear change in the solution as a function of α, but only in the vicinity of α^*. Note that the term in parentheses represents the Jacobian matrix elements of equation (7). The Jacobian thus plays a significant role, both in establishing the continuity of the solution branch and in Newton's iteration process. As long as $\mathbf{J}$ is non-singular, one can compute the tangents $\partial\eta_k/\partial\alpha$'s and examine the continuity of the branch given $\partial G_i/\partial\alpha$, $i = 1, \ldots, 2N$. In order to obtain these values, we need to define some more variables, say $\psi_i(\tau)$, its associated governing equations and the initial conditions; this set must be used along with the shooting procedure described earlier in Section 2.1:

$$\psi_i(\tau) = \partial q_i(\tau)/\partial\alpha, \qquad i = 1, \ldots, 2N, \tag{16}$$

$$\psi_i'(\tau) = \frac{\partial}{\partial\tau}\left\{\frac{\partial q_i(\tau)}{\partial\alpha}\right\} = \frac{\partial}{\partial\alpha}\left\{\frac{\partial q_i(\tau)}{\partial\tau}\right\} = \sum_{k=1}^{2N} \frac{\partial F_i}{\partial q_k}\psi_k + \frac{\partial F_i}{\partial\alpha}, \qquad i = 1, \ldots, 2N, \tag{17}$$

$$\psi_i(0) = 0, \qquad \forall\, i \; i \in [1, 2, \ldots, 2N]. \tag{18}$$

Comparing equations (15) and (16), we note that $\partial G_i/\partial\alpha = \psi_i(\tau_0)$, $i = 1, \ldots, 2N$. From the calculated tangents at $\alpha = \alpha^*$, one can estimate $\boldsymbol{\eta}$ for a small change in the parameter, i.e., $\alpha^1 = \alpha^* + \Delta\alpha$, as shown below:

$$\eta_i^{1^*} = \eta_i^0 + \left.\frac{\partial \eta_i}{\partial \alpha}\right|_{\alpha^*} \Delta\alpha, \qquad \eta_i^{1^*} = \eta_i(\alpha^1), \quad i = 1, \ldots, 2N. \tag{19}$$

This estimate is used to start the Newton iteration procedure as follows:

$$\mathbf{J}\Delta\boldsymbol{\eta}^{(k+1)} = -\mathbf{G}(\boldsymbol{\eta}^k; \alpha^1), \qquad k = 1, 2, \ldots\ . \tag{20}$$

This procedure works fine until $\mathbf{J}$ becomes singular, which is usually due to a *turning point* ($\lambda_i = +1$), as depicted in Figure 2(a). Such a situation occurs when $\partial\eta_k/\partial\alpha \to \infty$ for some k, or $\partial\Phi_k/\partial\alpha \notin \mathscr{R}(\mathbf{J})$, where $\mathscr{R}(\mathbf{J})$ denotes the range space of the Jacobian matrix. When $\lambda_i = -1$, the Jacobian is still non-singular for the regular Poincaré map ($m = 1$), but has a period-doubling turning point, as seen in Figure 2(b), for the double Poincaré map ($m = 2$), leading to an eigenvalue $\lambda_{i,m=2} = \lambda^2_{i,m=1} = 1$. The turning point as shown in Figure 2(a) can be handled quite easily, as it is essentially a problem of parametrization (see Figure 2(c)). We re-parameterize by introducing a new parameter, say arc length s, so that $\eta_i \equiv \eta_i(s)$, $\alpha \equiv \alpha(s)$ ($i = 1, \ldots, 2N$). Then, equation (15) is re-written as

$$\sum_{k=1}^{2N} \left\{\frac{\partial \Phi_i}{\partial \eta_k} - \delta_{ik}\right\} \frac{\partial \eta_k}{\partial s} + \frac{\partial G_i}{\partial \alpha}\frac{\partial \alpha}{\partial s} = 0. \qquad i = 1, \ldots, 2N. \tag{21}$$

We have, however, introduced one more unknown and in order to have the same number of equations as there are unknowns, we define the arc length equation as [19, 21]

$$\sum_{k=1}^{2N} \left(\frac{\partial \eta_k}{\partial s}\right)^2 + \left(\frac{\partial \alpha}{\partial s}\right)^2 = 1. \tag{22}$$

At the turning point, we re-write equation (21) as follows, which renders the modified Jacobian $\mathbf{J}^* = [\partial\mathbf{G}/\partial\boldsymbol{\eta} | \partial\mathbf{G}/\partial\alpha]$ non-singular:

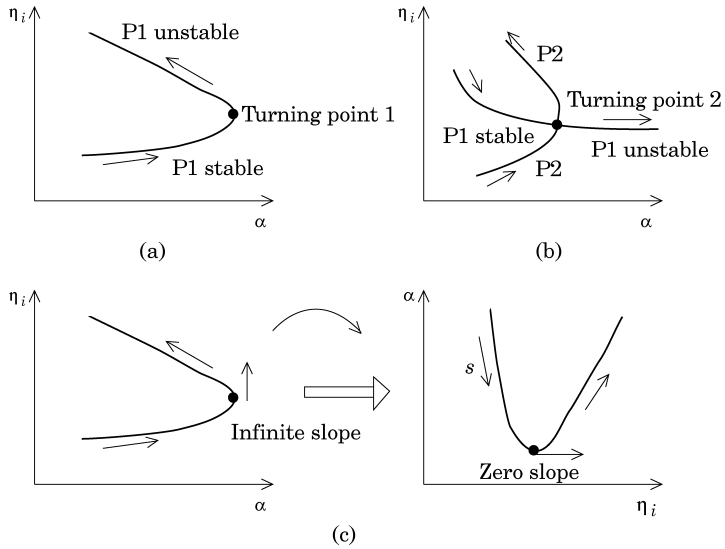

Figure 2. The two types of singularities on tracing a solution branch: (a) simple P1 turning point; (b) turning point on a P2 branch; (c) a geometric interpretation of arc length parametrization to go around the turning point.

$$\sum_{\substack{k=1\\k\neq m}}^{2N}\left\{\frac{\partial \Phi_j}{\partial \eta_k}-\delta_{jk}\right\}\frac{\partial \eta_k}{\partial s}+\frac{\partial G_j}{\partial \alpha}\frac{\mathrm{d}\alpha}{\mathrm{d}s}=-\left\{\frac{\partial \Phi_j}{\partial \eta_m}-\delta_{jm}\right\}\frac{\partial \eta_m}{\partial s}, \qquad j=1,\ldots,2N. \tag{23}$$

At the turning point, there is a change in the direction of the parameter α. If $\Delta\alpha$ was positive (negative) to begin with, then past the turning point $\Delta\alpha$ becomes negative (positive). In this manner, starting from an initial fixed point calculated as outlined in section 2.1, the procedure described above (termed *continuation*) can be carried out for any parameter range, with its unique ability of going around the turning points and tracing out the entire branch of fixed point solutions; see references [19, 21, 26]. Period-doubling branches, say P2 (period $2\tau_0$), which bifurcates from the P1 (period τ_0) branch, can be traced in a similar fashion once the initial P2 fixed point has been obtained using the regular shooting procedure of section 2.1, with $m = 2$. A repeated use of this procedure will yield P4 and other higher period solutions. The stability of the solutions is then examined using the monodromy matrix, **B** (see section 2.1.2). A uniform step size can be used over the whole parametric range, but this makes the process computationally inefficient. Several step size control algorithms exist [26, 27]; an algorithm based on an error estimation criterion, developed by Den Heijer and Rheinboldt [27], is used in our study.

3. APPLICATION TO DUFFING OSCILLATOR

The technique developed in section 2 is illustrated and validated by applying it to a commonly used single-degree-of-freedom (SDOF) Duffing oscillator, the governing equation of which is written in the format of equation (2) as

$$\begin{Bmatrix} q_1' \\ q_2' \end{Bmatrix} = \begin{bmatrix} 0 & 1 \\ -k & -\xi \end{bmatrix}\begin{Bmatrix} q_1 \\ q_2 \end{Bmatrix} + \begin{Bmatrix} 0 \\ -\beta q_1^3 \end{Bmatrix} + \begin{Bmatrix} 0 \\ f\cos(\Omega\tau) \end{Bmatrix}, \tag{24}$$

where k is the linear stiffness, ξ is the viscous damping coefficient, β is the non-linear stiffness coefficient, f is the external sinusoidal excitation amplitude and Ω is the excitation frequency. The variational equations defining $\mu_{ij}(\tau)$, $i, j = 1, \ldots, 2N$, can be obtained from equations (10) and (24) as

$$\begin{bmatrix} \mu_{11}' & \mu_{12}' \\ \mu_{21}' & \mu_{22}' \end{bmatrix} = \begin{bmatrix} 0 & 1 \\ -k-3\beta q_1^2 & -\xi \end{bmatrix}\begin{bmatrix} \mu_{11} & \mu_{12} \\ \mu_{21} & \mu_{22} \end{bmatrix}. \tag{25}$$

Similarly, the governing equations for $\psi_i(\tau)$ can be obtained from equations (17) and (24), when the parameter α is either the frequency Ω or the external excitation amplitude f respectively, as

$$\begin{Bmatrix} \psi_1' \\ \psi_2' \end{Bmatrix} = \begin{bmatrix} 0 & 1 \\ -k-3\beta q_1^2 & -\xi \end{bmatrix}\begin{Bmatrix} \psi_1 \\ \psi_2 \end{Bmatrix} + \begin{Bmatrix} 0 \\ -f\tau\sin(\Omega\tau) \end{Bmatrix}, \tag{26a}$$

$$\begin{Bmatrix} \psi_1' \\ \psi_2' \end{Bmatrix} = \begin{bmatrix} 0 & 1 \\ -k-3\beta q_1^2 & -\xi \end{bmatrix}\begin{Bmatrix} \psi_1 \\ \psi_2 \end{Bmatrix} + \begin{Bmatrix} 0 \\ \cos(\Omega\tau) \end{Bmatrix}. \tag{26b}$$

Now, by using equations (24)–(26) and the procedure developed in section 2, Figure 3 can be obtained, which shows a plot of the variation of the fixed points $q_i(0)$, $i = 1, 2$, as a function of Ω for $k = -0{\cdot}2$, $\xi = 0{\cdot}04$, $\beta = 8/15$ and $f = 0{\cdot}4$. This example has already been analyzed by Seydel [21] and, hence, it represents a test of the methodology developed here. The figure represents the subharmonic loop (P2) and contains stable and unstable solutions. As can be seen, our predictions match very well with Seydel's results [21].

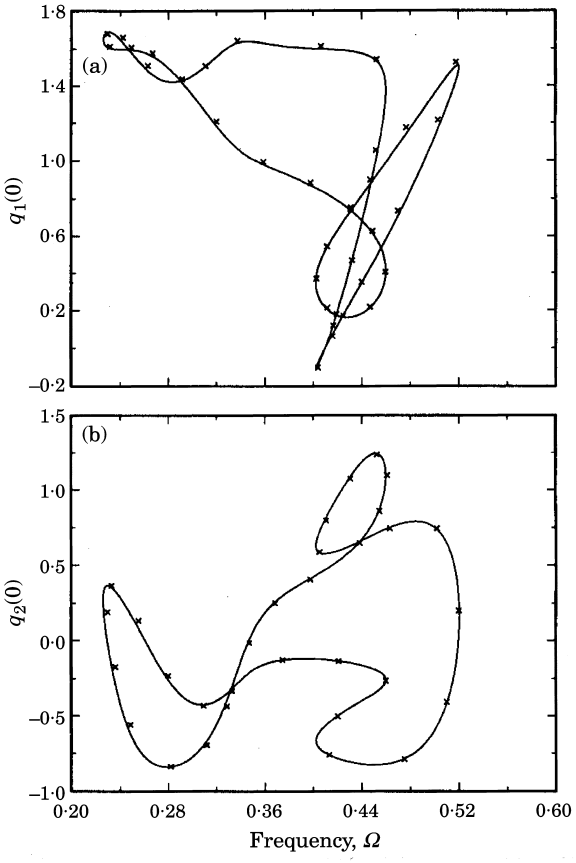

Figure 3. The subharmonic loop for the Duffing oscillator: ——, proposed scheme; ×, Seydel's scheme [21].

Next, the above equation is solved by using the continuation procedure (continuation parameter Ω) for three different sets of parameter values, as shown in Table 1. An initial fixed point is calculated, using the procedure in section 2.1, at a high frequency value, say $\Omega = 2$ or 2·5, where the non-linear effects are negligible, and then the continuation procedure, described in section 2.2, is started with an initial downward frequency sweep, i.e., $\Delta\Omega < 0$. The results are shown in Figures 4–6. These are compared with the predictions yielded by a one-term harmonic balance, which is obtained from the following cubic equation in terms of a^2, where a is the amplitude:

$$\tfrac{9}{16}\beta^2 a^6 + \tfrac{3}{2}\beta(k - \Omega^2)a^4 + \{(k - \Omega^2)^2 + \xi^2\Omega^2\}a^2 - f^2 = 0. \tag{27}$$

A first order perturbation scheme [28] leads to a similar equation, but is valid only for small β/k values. From Figure 4(a) one can see that our procedure yields excellent

TABLE 1

Parameter values used for the Duffing oscillator study, given $\xi = 0{\cdot}04$ *and* $f = 0{\cdot}30$

Figure	β	k	β/k
4(a)	0·10	1·0	0·10
4(b)	0·75	1·0	0·75
5 and 6	0·75	0·20	3·75

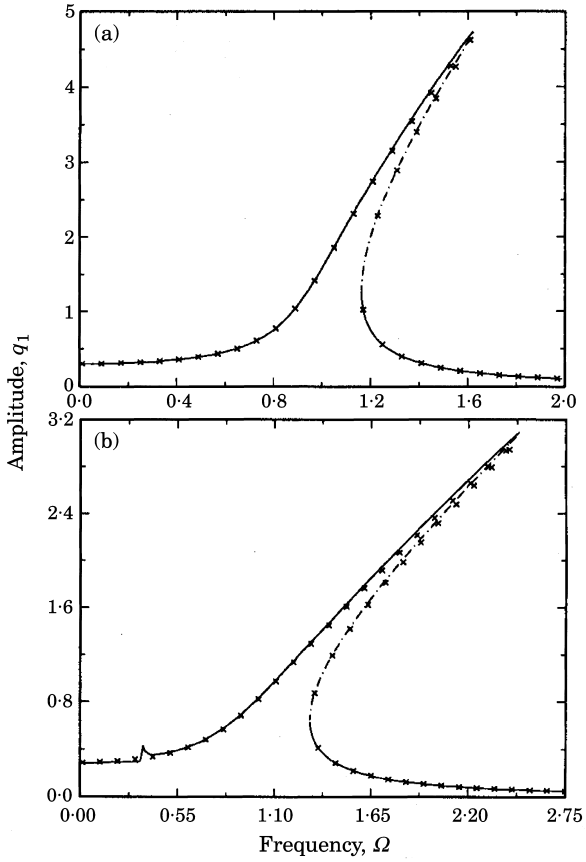

Figure 4. The frequency response of a hardening type Duffing oscillator: (a) weakly non-linear; (b) moderately non-linear system. ——, Stable; – · – · –, unstable (+1); ×, harmonic balance (one-term) solutions.

agreement with the harmonic balance or perturbation scheme. Note that there are two turning points, one near $\Omega = 1{\cdot}2$ and one near $\Omega = 1{\cdot}6$. When the continuation scheme goes around these points, the fixed points change from being stable (unstable) to unstable (stable) and $\Delta\Omega$ reverses signs. The three solutions regime (jump regions) predicted by both schemes are also in good agreement. Observe in Figure 4(b) that although the match between the semi-analytical and shooting method at most frequencies is still reasonable, the harmonic balance scheme cannot predict the superharmonic resonance at $\Omega \approx 0{\cdot}33$. This can obviously be remedied by introducing additional higher harmonics (such as order 3, 5, etc.) in the assumed solution, but the resulting equations are more complex than equation (27) and can only be solved by a Newton–Raphson type iteration scheme. When the linear stiffness is reduced, as in Figure 5, we note that the system becomes highly non-linear, especially at frequencies below $\Omega = 0{\cdot}50$, and the deviation between the one-term harmonic balance and the shooting method becomes significant. A number of super-harmonic resonances (of odd order 3, 5, 7, etc.) can be readily observed in Figure 5(b). Also, a symmetry breaking bifurcation phenomenon ($\lambda = +1$) is observed [29]. The asymmetric solution (P1) loop around the unstable symmetric P1 solutions is shown in Figure 6(a). This phenomenon is clarified by Figure 6(b), where the phase plane portrait is shown for the symmetric (unstable) as well as the asymmetric (stable) solutions for $\Omega = 0{\cdot}40$.

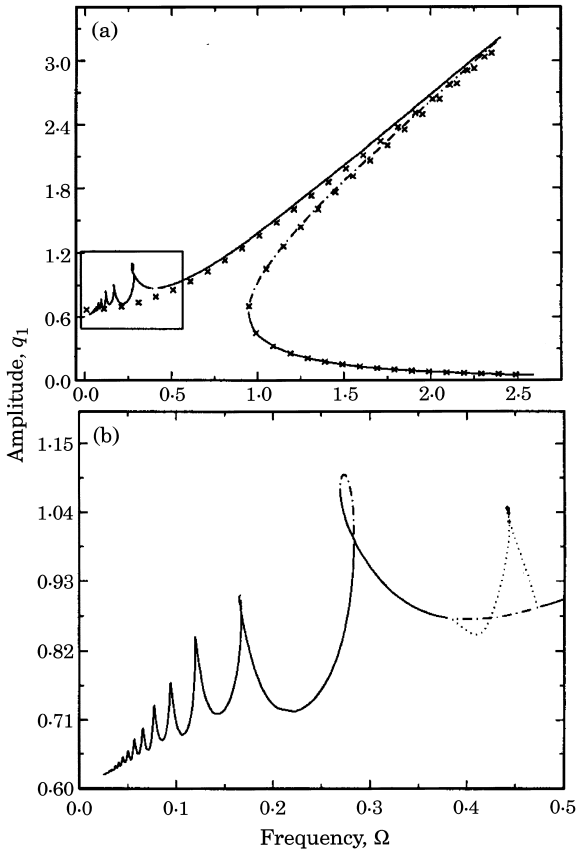

Figure 5. The frequency response of a strongly non-linear Duffing oscillator: (a) complete response; (b) expanded view of inset in (a). ——, Stable; – · – · –, unstable (+1); · · · · ·, stable (asymmetric); +, unstable (asymmetric); ×, harmonic balance (one-term) solutions.

4. ANALYSIS OF AN IMPACT PAIR

4.1. SINGLE HARMONIC EXCITATION

We re-investigate the specific impact pair problem analyzed earlier by Comparin and Singh [7], in order further to validate the proposed scheme, as well as to explain some of the analog computer simulation results that could not be explained in their investigation. The governing equations of the impact pair as shown in Figure 7 have been re-formulated as

$$I_1\ddot{x}_1 + C(\dot{x}_1 - \dot{x}_2) + K(x_1 - x_2) + (K_1 - K)g(q_1) = E_m + E_p \cos(\omega t), \tag{28}$$

$$I_2\ddot{x}_2 - C(\dot{x}_1 - \dot{x}_2) - K(x_1 - x_2) - (K_1 - K)g(q_1) = -E_m, \tag{29}$$

where $q_1 = x_1 - x_2$. Combining equations (25) and (26) and defining parameters $\zeta = C/2I\omega_n$, $\omega_n = \sqrt{K_1/I}$, $I = I_1I_2/(I_1 + I_2)$, $\kappa = K/K_1$, $\tau = \omega_n t$, $\Omega = \omega/\omega_n$, $e_m = E_m/I\omega_n^2$ and $e_p = E_p/I_1\omega_n^2$, we obtain

$$\begin{Bmatrix} q_1' \\ q_2' \end{Bmatrix} = \begin{bmatrix} 0 & 1 \\ -\kappa & -2\zeta \end{bmatrix} \begin{Bmatrix} q_1 \\ q_2 \end{Bmatrix} + \begin{Bmatrix} 0 \\ -g(q_1) \end{Bmatrix} + \begin{Bmatrix} 0 \\ e_m + e_p \cos(\Omega\tau) \end{Bmatrix}. \tag{30}$$

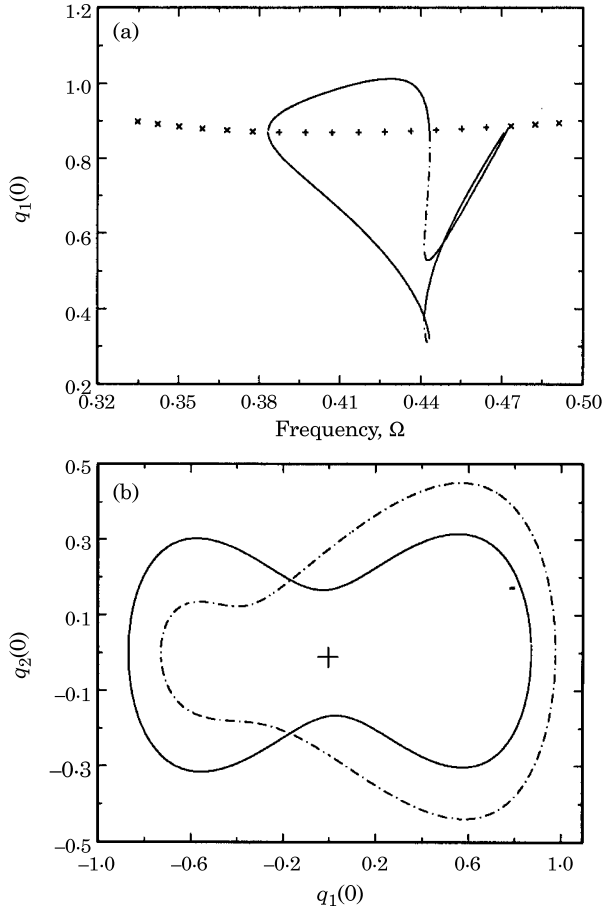

Figure 6. The symmetry-breaking bifurcation in a Duffing oscillator. (a) The fixed point loop of asymmetric solutions: ×, stable (symmetric); +, unstable (symmetric); ——, stable (asymmetric); – · – · –, unstable (asymmetric). (b) The phase plane, showing asymmetric and symmetric solutions at $\Omega = 0{\cdot}40$: ——, symmetric (unstable); – – – – –, asymmetric (stable) solutions.

The non-linear function $g(q_1)$ shown in Figure 7(b) is defined as

$$g(q_1) = \begin{cases} (1-\kappa)(q_1 - b_r), & q_1 > b_r, \\ 0, & -b_r \leqslant q_1 \leqslant b_r, \\ (1-\kappa)(q_1 + b_r), & q_1 < -b_r. \end{cases} \tag{31}$$

The variational equations defining μ_{ij}, and parametric equations (with parameters Ω and e_p, respectively) for ψ_i (with $i, j = 1, \ldots, 2N$) are obtained from equations (10), (17) and (30) as

$$\begin{bmatrix} \mu_{11}' & \mu_{12}' \\ \mu_{21}' & \mu_{22}' \end{bmatrix} = \begin{bmatrix} 0 & 1 \\ -\kappa - \mathrm{d}g(q_1) & -2\zeta \end{bmatrix} \begin{bmatrix} \mu_{11} & \mu_{12} \\ \mu_{21} & \mu_{22} \end{bmatrix}, \tag{32}$$

$$\begin{Bmatrix} \psi_1' \\ \psi_2' \end{Bmatrix} = \begin{bmatrix} 0 & 1 \\ -\kappa - \mathrm{d}g(q_1) & -2\zeta \end{bmatrix} \begin{Bmatrix} \psi_1 \\ \psi_2 \end{Bmatrix} + \begin{Bmatrix} 0 \\ -e_p \tau \sin(\Omega\tau) \end{Bmatrix}, \tag{33a}$$

$$\begin{Bmatrix} \psi_1' \\ \psi_2' \end{Bmatrix} = \begin{bmatrix} 0 & 1 \\ -\kappa - \mathrm{d}g(q_1) & -2\zeta \end{bmatrix} \begin{Bmatrix} \psi_1 \\ \psi_2 \end{Bmatrix} + \begin{Bmatrix} 0 \\ \cos(\Omega\tau) \end{Bmatrix}, \tag{33b}$$

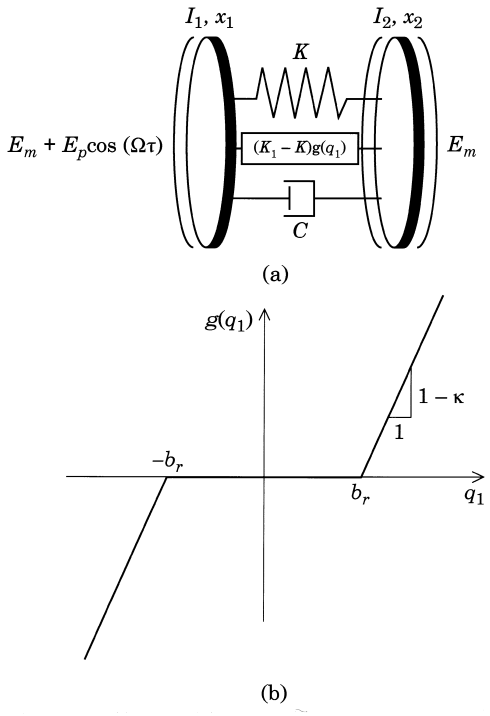

Figure 7. The model of an impact pair [7]: (a) the two-degree-of-freedom semi-definite system; (b) the clearance non-linearity ($q_1 = x_1 - x_2$).

$$\mathrm{d}g(q_1) = \frac{\mathrm{d}g(q_1)}{\mathrm{d}q_1} = \begin{cases} (1-\kappa), & q_1 > b_r, \\ 0, & -b_r \leqslant q_1 \leqslant b_r, \\ (1-\kappa), & q_1 < -b_r. \end{cases} \tag{34}$$

The system of given equations (30)–(34) is solved by using the proposed continuation procedure and the results are shown in Figures 8–14. The values of the parameters used in the study are listed in Table 2. For the sake of illustration, the continuation parameter α used for all these studies was the non-dimensional excitation frequency Ω. Here again, the initial fixed point is obtained at a high frequency value, say $\Omega > 2{\cdot}0$, as the non-linear effects are small and the initial $\Delta\Omega$ is negative (downward sweep). For this system, the secondary Hopf bifurcation phenomenon is not observed, which can be established by Liouville's theorem [18].

In Figure 8(a), the frequency response is plotted for a heavily loaded impact pair. Since $\kappa = 0$, this represents a backlash problem. The analog computer results from reference [7] are shown in the figure for comparison, and an excellent agreement between the proposed

TABLE 2

Parameters used in this study of the impact pair, given $b_r = 1$

Figures	ζ	κ	e_m	e_p	e_p/e_m
8 and 11(a)	0·015	0·0	0·50	0·25	0·50
9 and 12	0·015	0·25	0·25	0·25	1·0
10 and 11(b)	0·015	0·50	0·25	0·25	1·0
13, 14 and 15	0·03	0·0	0·25	0·50	2·0

procedure and analog simulation is evident, especially with respect to the jump transitions. The classic jump phenomenon observed corresponds to saddle-node bifurcations ($\lambda = +1$). The jumps, unlike the Duffing oscillator, occur at two different regions due to the presence of a mean load. The two saddle-node bifurcations at the lower frequency region, as evident from Figure 8(b), corresponds to a transition from no-impact to single-sided impact and single-sided to double-sided impact, respectively [7], in the direction of increasing frequency. The other two saddle-node bifurcations correspond to transitions from stable P1 to unstable P1, with both undergoing double-sided impact, and from double-sided impact to single-sided impact, respectively, again in the direction of increasing frequency (see Figure 8(b)).

At this juncture it is appropriate to recall the motivation and methodology of analog computer simulation reported earlier in 1989 by Comparin and Singh [7]. It was carried out on a Comdyna GP-6 analog computer with a function generator for modelling the clearance non-linearity. The time domain output of the analog computer was suitably averaged to eliminate noise, using a digital analyzer (Nicolet UA 500). For a given excitation frequency Ω, the mean $q_{1,mean}$ and standard deviation $q_{1,amp}/\sqrt{2}$ of the time domain response were obtained using a digital oscilloscope (Data Precision 6000). The mean and standard deviation were calculated with all frequency components (sub- and superharmonics) of the response included. The emphasis of the analysis was on the prediction of the root mean square (r.m.s.) vibration level, and an extensive study of the

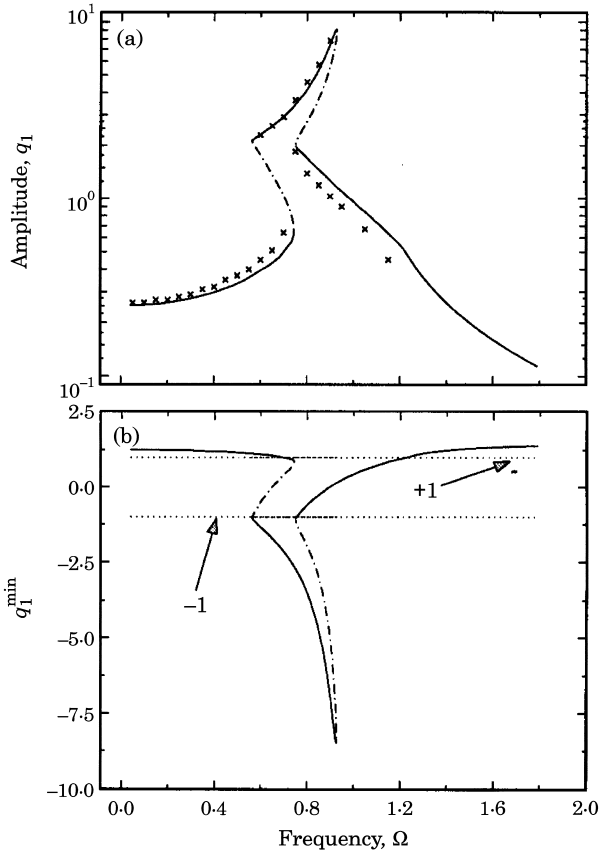

Figure 8. The response of a heavily loaded impact pair with $\kappa = 0$: (a) the complete frequency response; (b) impact transitions; ——, Stable; $- \cdot - \cdot - \cdot$, unstable $(+1)$; $\times$, analog simulation solutions.

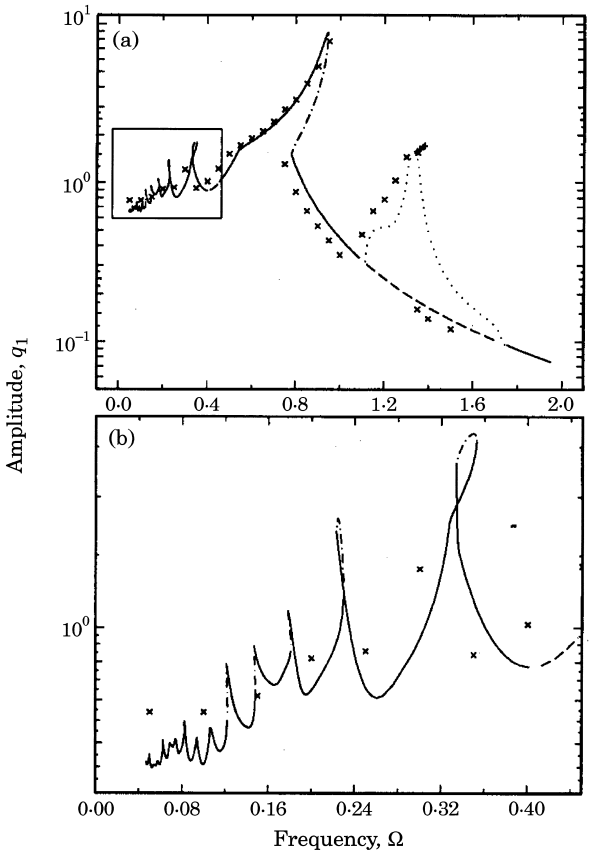

Figure 9. The response of a moderately loaded impact pair with $\kappa = 0{\cdot}25$: (a) the complete frequency response; (b) expanded view of inset in (a). ——, Stable; – · – · –, unstable (+1); – – – –, unstable (−1); · · · · ·, stable P2, +, unstable P2 (+1); ×, analog simulation solutions.

response for various initial conditions was not conducted. Due to the electronic limitations of the function generator, the transitions between the stiffness stages were slightly rounded, which may have affected where the jump points occurred. This was observed in some cases, especially for light mean loads e_m. Finally, the signal-to-noise ratio and signal saturation problems are invariably sources of error in an analog simulation. Hence, the analog simulation results of reference [7] must be viewed in the context of the above discussion. The analog simulation data is used here essentially as a qualitative tool for a comparison of various solution regimes as predicted by our proposed procedure.

When the mean load e_m is reduced, as in Figure 9 for $\kappa = 0{\cdot}25$, we can see that the resulting frequency response becomes more complex. A supercritical pitchfork bifurcation occurs resulting in unstable P1, but stable subharmonic P2 solutions in the region of $1{\cdot}12 \leqslant \Omega \leqslant 1{\cdot}74$. This subharmonic loop does not exhibit any further period-doubling bifurcations. Again, the analog computer simulation results are plotted for comparison, and now observe an excellent agreement except at the lower frequencies. In fact, some of the analog solutions are on the subharmonic loop, a fact that could not be explained earlier using the describing function approach [7]. At low frequencies, the shooting method predicts a number of superharmonic resonances, each with its saddle-node bifurcations, which were not predicted well by the analog simulation, possibly due to very coarse frequency spacing.

When κ is increased from 0·25 to 0·50, the results in Figure 10(a) show that the system tends to be more linear in its behavior. For instance, the subharmonic loop at the higher frequencies disappears. Also, the saddle-node bifurcations at the superharmonic resonances cease to exist. The analog simulation results again show good agreement with the proposed procedure and do predict fairly well the order 2 superharmonic resonant peak. In Figure 10(b), a three-dimensional picture of the variation of $q_i(0)$ with Ω is shown, specifically to understand how the fixed points evolve as the parameter value changes.

The continuation procedure is validated further by comparing results with those yielded by a multi-term harmonic balance or Galerkin scheme [30]. The main drawback of the harmonic balance scheme is that it cannot turn past the saddle-node bifurcations and trace the unstable (+1) P1 solutions. Otherwise, as can be seen in Figures 11 and 12, an excellent match between the harmonic balance and the proposed schemes is evident. For the heavily loaded ($e_p/e_m = 0{\cdot}50$) and the high κ ($=0{\cdot}50$) cases, shown in Figures 11(a) and (b), respectively, a small number of harmonic terms ($\leqslant 5$) is sufficient to achieve the required tolerance for the truncation error which is caused by neglecting higher harmonics in the trigonometric expansion. However, for the low frequency results shown in Figure 12, which correspond to $\kappa = 0{\cdot}25$ and $e_p/e_m = 1{\cdot}0$, a fairly large number of harmonics (about

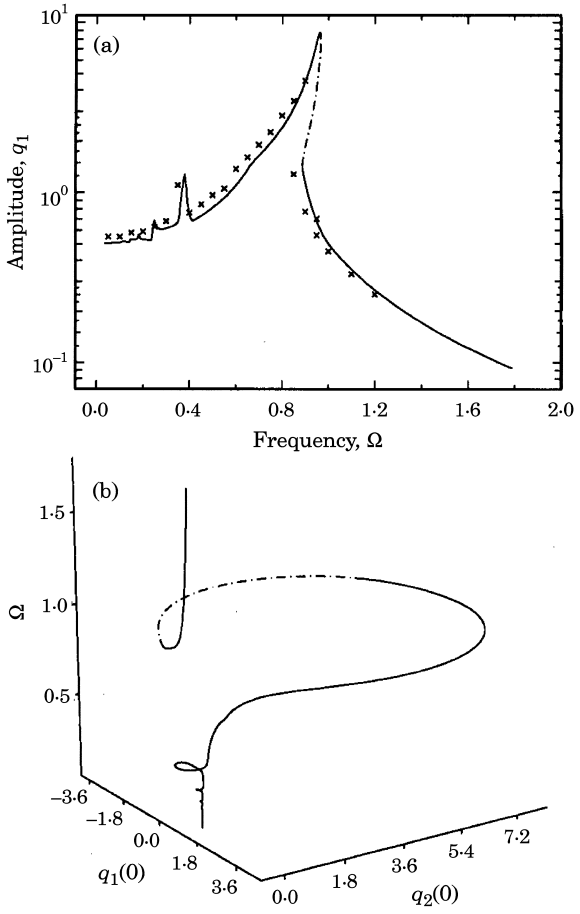

Figure 10. The response of a moderately loaded impact pair with $\kappa = 0{\cdot}50$: (a) the frequency response; (b) the evolution of the Poincaré map as Ω changes. ——, Stable; – · – · –, unstable (+1); ×, analog simulation solutions.

15–20) must be included to meet the truncation error tolerance. This implies that the size of the matrices involved in the iteration process becomes very large. Also, in order to determine the stability of the solutions, one needs to construct a monodromy matrix based on Floquet theory [25]. For this purpose, a sufficient number of harmonics must be included to determine stability transitions with reasonable accuracy. This makes the harmonic balance scheme computationally inefficient when the system is lightly loaded and/or has a low κ value, especially at low frequencies. The proposed procedure does not suffer from such a restriction.

The final example case deals with a lightly loaded system; here the amplitude of the sinusoidal excitation is twice the mean load. As seen in Figure 13, there is again a supercritical pitchfork bifurcation leading to subharmonic solutions. At the low frequencies, pitchfork and saddle-node bifurcations also occur near most superharmonic resonances. The main pitchfork loop, which is clearly asymmetric about the unstable P1 solutions, is shown in Figure 14. The pitchfork bifurcation, at the high frequency region, exhibits further period-doubling bifurcations leading to P4, P8, P16 solutions and so on. These are not shown in these figures for clarity. This phenomenon signals the possible occurrence of chaos in this region. Direct numerical integration, with initial conditions slightly perturbed from one of the high period solutions, do however confirm the presence

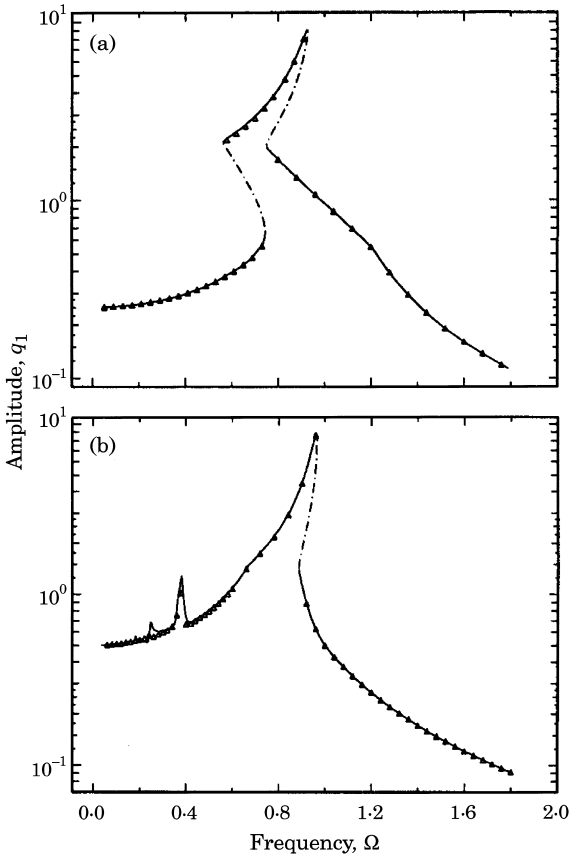

Figure 11. A comparison of the proposed scheme with a harmonic balance scheme: (a) heavily loaded case with $\kappa = 0$; (b) moderately loaded case with $\kappa = 0{\cdot}50$. ——, Stable; – · – · –, unstable (+1), △, multi-term harmonic balance solutions.

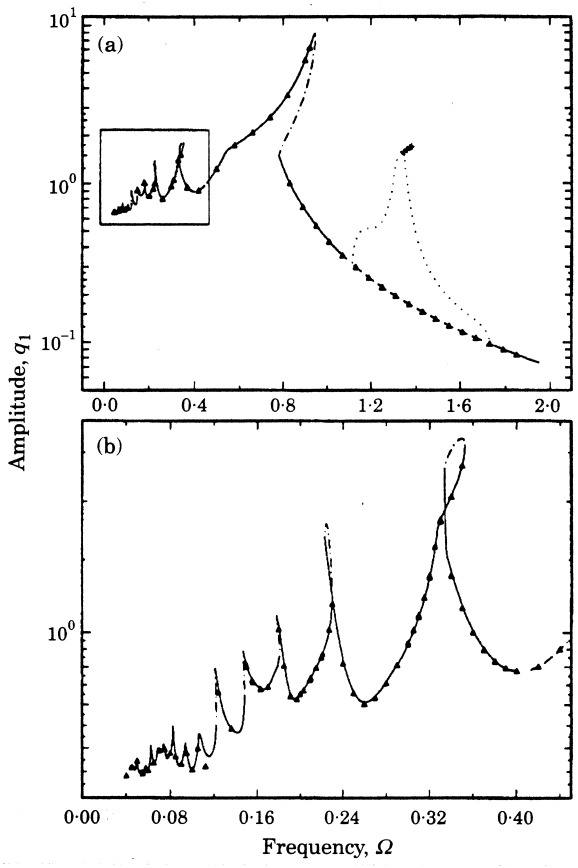

Figure 12. A comparison of the proposed scheme with a harmonic balance method for a moderately loaded impact pair with $\kappa = 0{\cdot}25$: (a) the complete frequency response; (b) expanded view of inset in (a). ——, Stable; – · – · –, unstable (+1); – – – –, unstable (−1); · · · · ·, stable P2; +, unstable P2 (+1); △, multi-term harmonic balance solutions.

of chaos in this region. For example, in Figure 15 are shown the time history, the Fourier spectrum and the Poincaré section, for $\Omega = 1{\cdot}1$. It is clear from the fractal nature of the Poincaré section and the broad-band spectrum that the solution is indeed chaotic.

Finally, we summarize some of the response characteristics of the impact pair problem. When the impact pair is heavily loaded ($e_p/e_m < 1$) and/or has high κ, the system does not exhibit subharmonic or non-periodic solutions. However, when the mean load is reduced, the high frequency region has stable subharmonic (P2 and higher period) solutions just above the primary resonance. Chaotic solutions can also occur due to period-doubling bifurcations, especially when e_p/e_m is greater than 1·25. The frequency response becomes most complex at the lower frequencies, since there is a strong possibility of subharmonic and non-periodic solutions over most of the low frequency range.

4.2. COMPUTATIONAL ISSUES

In order to demonstrate the potential savings in computational effort, typical CPU times are compared in Table 3 (on the same basis) for two example cases corresponding to Figures 8 and 13 (see Table 2 for the parameters used) for the results obtained by direct numerical integration and the proposed continuation. Clearly, the CPU time for the

TABLE 3

A comparison of classical numerical integration with the continuation method

Issue	Classical integration	Continuation
Multi-valued and unstable solutions	Large initial condition map needs to be searched; unstable solutions can be obtained only by integration in negative time	Initial point alone needs some effort; other points obtained quite efficiently, including subharmonic and unstable solutions
Example case	CPU times for 250 parameter points:	
(a) Figure 8	3000 s	185 s
(b) Figure 13	7400 s	295 s

continuation procedure is at least an order of magnitude smaller than that required for classical numerical integration. This is primarily because the direct numerical integration procedure needs to be carried out for several time periods of the excitation, in order to achieve steady state conditions. Note that in order to obtain the unstable results by direct numerical integration one has to integrate in negative time as well. Also, in order to find

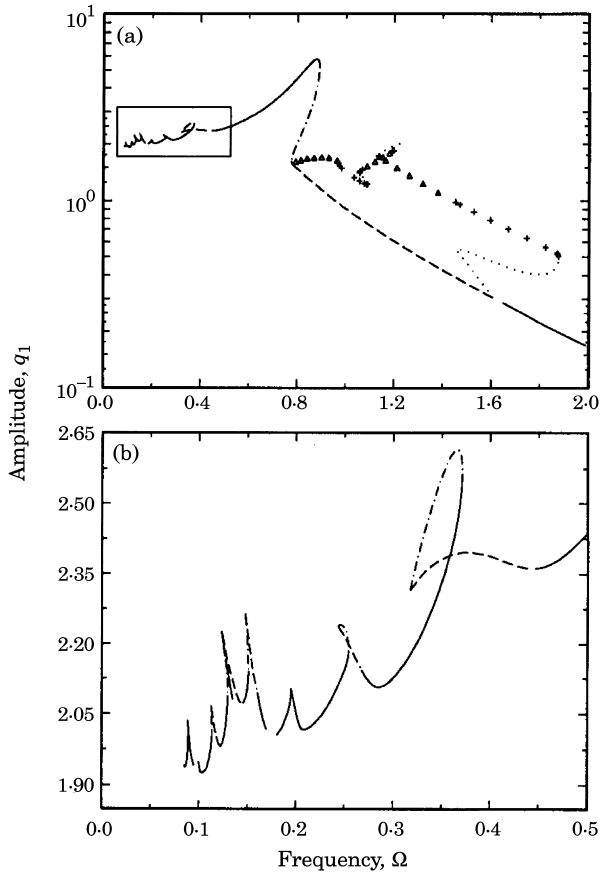

Figure 13. The frequency response for a lightly loaded impact pair for $\kappa = 0$: (a) the complete response; (b) expanded view of the inset in (a). ——, Stable; – · – · –, unstable (+1); – – – –, unstable (−1); · · · · ·, unstable P2 (+1); +, stable P2; △, unstable P2 (−1) solutions.

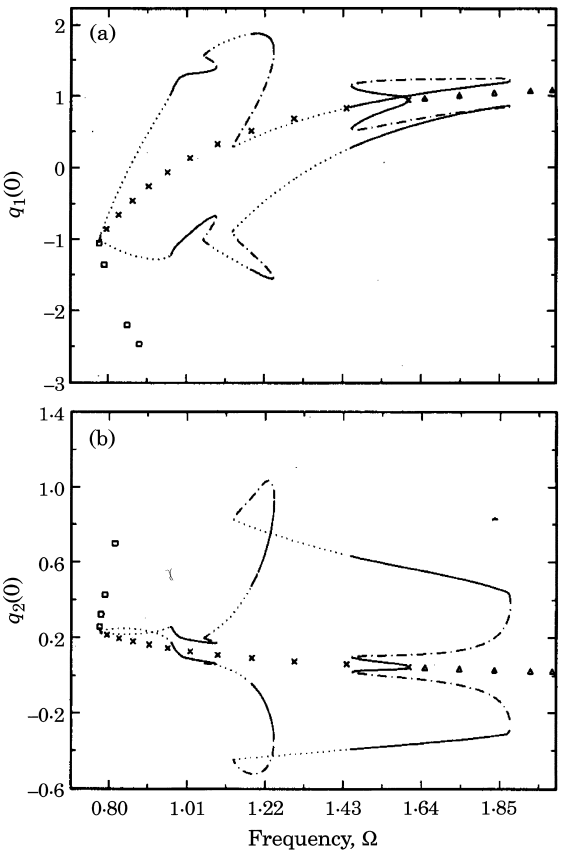

Figure 14. The subharmonic fixed point solution loop for a lightly loaded impact pair with $\kappa = 0$: (a) $q_1(0)$ versus Ω; (b) $q_2(0)$ versus Ω. ——, Stable P2; $-\cdot-\cdot-\cdot-$, unstable P2 $(+1)$; $\cdots\cdots$, unstable P2 (-1); $\triangle$, stable P1; $\square$, unstable P1 $(+1)$; $\times$, unstable P1 (-1) solutions.

subharmonic, quasi-periodic or chaotic solutions, a large initial condition map must be searched, since we do not have an *a priori* knowledge of which parameter regions exhibit such phenomena. Conversely, in the proposed procedure, such regimes are found more efficiently. For example, the occurrence of a period-doubling bifurcation during the continuation process ($\lambda = -1$) signals the possible occurrence of stable P2, higher period subharmonic solutions or even chaotic solutions through the Feigenbaum cascade [19, 21]. Using values of $m = 2$, 4, etc., in the method described in section 2, one can then obtain the subharmonic solutions and the period-doubling cascade. Similar procedures may also be established for other types of solutions.

4.3. MULTI-HARMONIC EXCITATION

In the previous sections, all of the example cases were for a single harmonic excitation only. However, the formulation developed in section 2 is valid for any periodic excitation that can be represented by a Fourier series in terms of the fundamental excitation frequency Ω. To illustrate this point, we consider one example of a multi-harmonic excitation of the impact pair. In equation (29), the term $e_p \cos(\Omega\tau)$ is replaced by $\sum_{k=1}^{M} e_{p_k} \cos(k\Omega\tau)$, where M is the number of harmonics in the excitation. The system

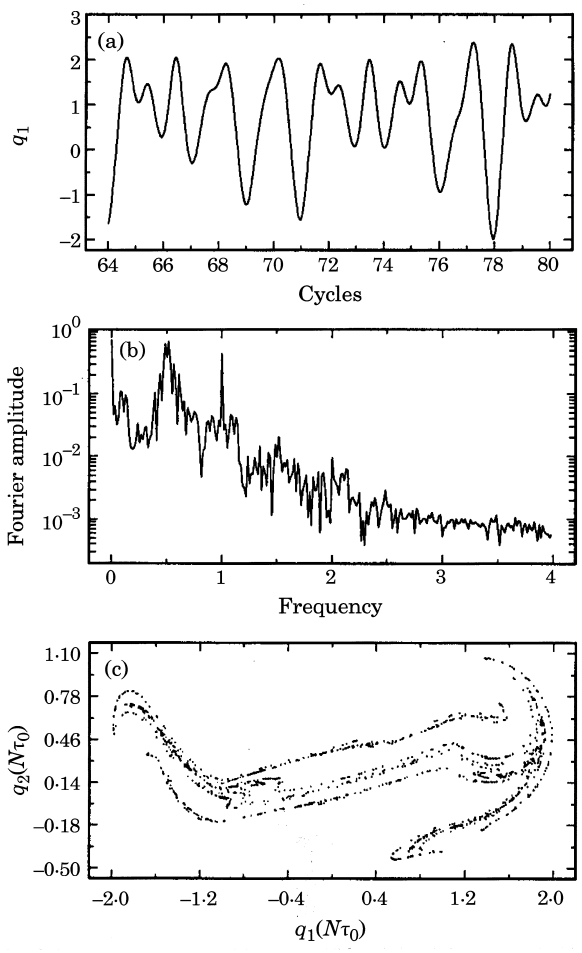

Figure 15. The occurrence of a chaotic solution through period-doubling for the lightly loaded impact pair: (a) time history; (b) Fourier spectrum; (c) Poincaré section when $\Omega = 1{\cdot}1$.

corresponding to Figure 8 (see Table 2) is simulated again with the external excitation parameters set to $e_m = 0{\cdot}50$, $e_{p_1} = 0{\cdot}25$, $e_{p_2} = 0{\cdot}10$ and $e_{p_3} = 0$ in Figure 16(a), and to $e_m = 0{\cdot}50$, $e_{p_1} = 0{\cdot}25$, $e_{p_2} = 0{\cdot}10$ and $e_{p_3} = 0{\cdot}05$ in Figure 16(b), respectively. A comparison of Figures 16 and 8(a) shows that the presence of the additional harmonics does not change the frequency response significantly for frequencies above $\Omega = 0{\cdot}8$. However, at the lower frequencies, the second and third superharmonic resonances are excited and the peak amplitudes are of the same order of magnitude as the one associated with the primary resonance. Note that the addition of the third harmonic excitation does not change the response above $\Omega = 0{\cdot}40$. However this, may not be the case for lightly loaded situations, where significant dynamic interactions may be anticipated.

5. CONCLUDING REMARKS

This paper has adapted a parametric continuation scheme, based on the shooting method, specifically to analyze the dynamics of a piecewise non-linear system. It represents a fundamental attempt at clarifying the effect of various system or excitation parameters

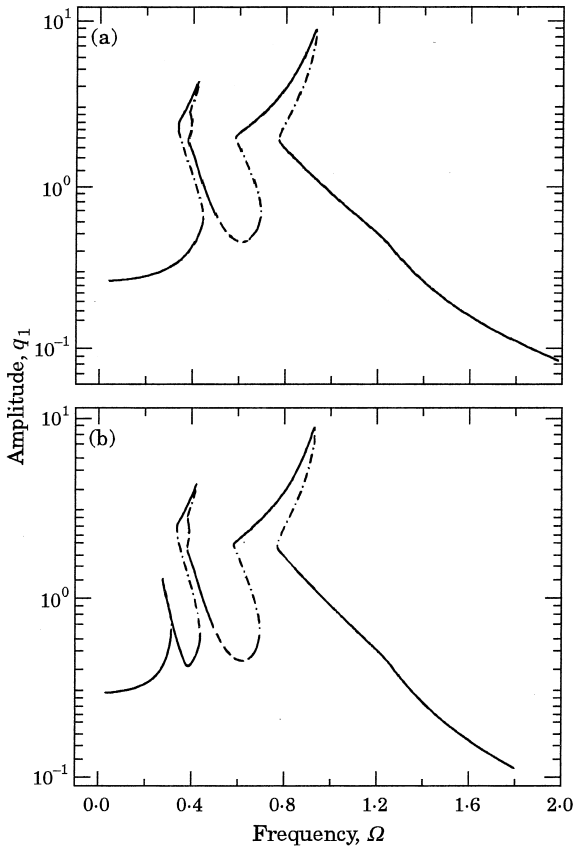

Figure 16. The frequency response of a heavily loaded oscillator with $\kappa = 0$ for multi-harmonic excitation (a) two harmonic excitation; (b) three harmonic excitation. ——, Stable; – · – · – ·, unstable (+1); – – – –, unstable (−1) solutions.

on the steady state response of the system irrespective of the nature of the non-linearity. We believe that we have developed a systematic way to find parameter regimes in which jump phenomena, subharmonic and chaotic solutions can occur, which was not previously possible using some of the other available techniques in the literature. This is the most significant contribution of this paper. Guidelines for the effective use of this method have been provided. Although only single-degree-of-freedom (SDOF) systems have been illustrated, the technique works quite well for higher DOF models and can be modified for conducting optimization studies. However, the developed procedure has limitations in its application to non-linear systems of very large dimension, because of the tremendous increase in the total number of variational equations. The quasi-Newton schemes, which lead to a reduction in the size of the equations, do not approximate the Jacobian well enough to yield reasonably accurate estimates of the stability transitions [26]. Hence, there is a clear need to refine these methods to make them more suitable for studying large dimension systems. For instance, numerical difficulties arising due to the stiff nature of the governing equations need to be resolved [31, 32]. Future work is being directed towards such issues in the context of multi-degree-of-freedom piecewise non-linear systems subject to multi-harmonic excitations.

ACKNOWLEDGMENTS

The authors wish to acknowledge the primary support from the U.S. Army Research Office (URI Grant DAAL 03-92-G-0120; 1992–97; Project Monitor Dr T. L. Doligalski), as well as additional support from the Nissan Technical Center (Japan) and the Center for Automotive Research at The Ohio State University. The first author is indebted to Professor G. R. Baker of The Ohio State University for introducing him to the techniques used in this paper. Thanks are also due to Dr R. J. Comparin for sharing the analog computer results.

REFERENCES

1. K. Karagiannis and F. Pfeiffer 1991 *Nonlinear Dynamics* **2**, 367–387. Theoretical and experimental investigations of gear-rattling.
2. J. Shaw and S. W. Shaw 1989 *Transactions of the American Society of Mechanical Engineers, Journal of Applied Mechanics* **56**, 168–174. The onset of chaos in a two-degree-of-freedom impacting system.
3. H. S. Choi and J. Y. K. Lou 1991 *International Journal of Nonlinear Mechanics* **26**, 461–473. Nonlinear behavior and chaotic motions of an SDOF system with piecewise-nonlinear stiffness.
4. Y. B. Kim and S. T. Noah 1991 *Transactions of the American Society of Mechanical Engineers, Journal of Applied Mechanics* **58,** 545–553. Stability and bifurcation analysis of oscillators with piecewise-linear characteristics: a general approach.
5. C. W. Wong, W. S. Zhang and S L. Lau 1991 *Journal of Sound and Vibration* **149**, 91–105. Periodic forced vibration of unsymmetric piecewise-linear systems by incremental harmonic balance method.
6. M. Kataoka, S. Ohno and T. Sugimoto 1991 *Japan Society of Mechanical Engineers, International Journal Series III* **34**, 345–354. Forced torsional vibration of a two-degree-of-freedom system including a clearance and two-step-hardening spring.
7. R. J. Comparin and R. Singh 1989 *Journal of Sound and Vibration* **134**, 259–290. Non-linear frequency response characteristics of an impact pair.
8. M. A. Veluswami and F. R. E. Crossley 1975 *Transactions of the American Society of Mechanical Engineers, Journal of Engineering for Industry* **97**, 820–827. Multiple impacts of a ball between two plates, part 1: some experimental observations.
9. M. A. Veluswami, F. R. E. Crossley and G. Horvay 1975 *Transactions of the American Society of Mechanical Engineers, Journal of Engineering for Industry* **97**, 828–835. Multiple impacts of a ball between two plates, part 1: some mathematical modeling.
10. R. Singh, H. Xie and R. J. Comparin 1989 *Journal of Sound and Vibration* **131**, 177–196. Analysis of automotive neutral gear rattle.
11. A. Kahraman and R. Singh 1991 *Journal of Sound and Vibration* **144**, 469–506. Non-linear dynamics of a geared rotor-bearing system with multiple clearances.
12. R. J. Comparin and R. Singh 1990 *Journal of Sound and Vibration* **142**, 101–124. Frequency response characteristics of a multi-degree-of-freedom system with clearances.
13. M. Urabe and A. Reiter 1966 *Journal of Mathematical Analysis and Applications* **14**, 107–140. Numerical computation of nonlinear forced oscillations by Galerkin's procedure.
14. A. Gelb and W. E. Vander Velde 1968 *Multiple-Input Describing Functions and Nonlinear Systems Design*. New York: McGraw-Hill.
15. F. H. Ling 1983 *Applied Mathematics and Mechanics* (English edition) **4**, 525–546. A numerical treatment of the periodic solutions of non-linear vibration systems.
16. S. Foale and J. M. T. Thompson 1991 *Computer Methods in Applied Mechanics and Engineering* **89**, 381–394. Geometrical concepts and computational techniques of nonlinear dynamics.
17. J. Awrejcewicz and T. Someya 1991 *Journal of Sound and Vibration* **146**, 527–532. Periodic, quasi-periodic and chaotic orbits and their bifurcations in a system of coupled oscillators.
18. K. Sato, S. Yamamoto and T. Kawakami 1991 *Computational Mechanics* **7**, 173–182. Bifurcation sets and chaotic states of a gear system subject to harmonic excitation.
19. M. Kubícek and M. Marek 1983 *Computational Methods in Bifurcation Theory and Dissipative Structures*. New York: Springer-Verlag.
20. M. Holodniok and M. Kubícek 1984 *Journal of Computational Physics* **55**, 254–267. DERPER—an algorithm for continuation of periodic solutions in ordinary differential equations.

21. R. Seydel 1988 *From Equilibrium to Chaos: Practical Bifurcation and Stability Analysis*. New York: Elsevier.
22. J. R. Dormand and P. J. Prince 1978 *Celestial Mechanics* **18**, 223–232. New Runge–Kutta algorithms for numerical simulation in dynamical astronomy.
23. C. G Broyden 1969 *Computer Journal* **12**, 94–99. A new method of solving non-linear simultaneous equations.
24. M. R. Matausek 1976 *Journal of Optimization Theory and Applications* **20**, 37–46. On Warner's algorithm for the solution of boundary-value problems for ordinary differential equations.
25. G. Iooss and D. D. Joseph 1980 *Elementary Stability and Bifurcation Theory*. New York: Springer-Verlag.
26. E. L. Allgower and K. Georg 1990 *Numerical Continuation Methods: an introduction*. New York: Springer-Verlag.
27. C. Dan Heijer and W. C. Rheinboldt 1981 *SIAM Journal of Numerical Analysis* **18**, 925–948. On steplength algorithms for a class of continuation methods.
28. A. H. Nayfeh and D. T. Mook 1979 *Nonlinear Oscillations*. New York: John Wiley.
29. J. Miles 1989 *SIAM Journal of Applied Mathematics* **49**, 968–981. Resonance and symmetry breaking for a Duffing oscillator.
30. F. H. Ling and X. X. Wu 1987 *International Journal of Nonlinear Mechanics* **22**, 89–98. Fast Galerkin method and its application to determine periodic solutions of non-linear oscillators.
31. E. Hairer, S. P. Norsett and G. Wanner 1987 *Solving Ordinary Differential Equations II—Stiff Problems*. Berlin: Springer-Verlag.
32. C. Padmanabhan, R. C. Barlow, T. E. Rook and R. Singh 1995 *American Society of Mechanical Engineers, Journal of Mechanical Design* **117,** 185–192. Computational Issues Associated with Gear Rattle Analysis.

APPENDIX A: LIST OF SYMBOLS

a	sinusoidal amplitude term for Duffing oscillator
$\mathbf{A}$	linear state matrix
b_r	transition from first to second stage stiffness of the impact pair
$\mathbf{B}$	monodromy matrix
C	viscous damping for the impact pair
e	normalized excitation force on impact pair
E	excitation force on the impact pair
f	excitation amplitude for Duffing oscillator
$\mathbf{F}$	general force vector
g	non-linear force function for the impact pair
$\mathbf{G}$	general non-linear function vector
$\mathbf{h}$	general non-linear force vector
I_1	first inertia of the impact pair
I_2	second inertia of the impact pair
I	combined inertia term for the impact pair
$\mathbf{J}$	Jacobian matrix
k	linear stiffness term for Duffing oscillator
K	first stage stiffness of the impact pair
K_1	second stage stiffness of the impact pair
M	number of excitation harmonics
N	number of degrees of freedom of any system
$\mathbf{q}$	state vector
s	arc length parameter
$\mathbf{T}$	external excitation vector
x_i	displacements of impact pair; $i = 1, 2$
α	parameter
α^*	parameter value at fixed point
β	cubic stiffness coefficient for Duffing oscillator
δ	Kronecker delta
$\mathbf{\Phi}$	state vector magnitude at τ_0
κ	ratio of the first and second stage stiffness for the impact pair
λ	eigenvalue of monodromy matrix

θ homotopy parameter
$\boldsymbol{\mu}$ derivative matrix of the state vector with respect to (w.r.t.) $\boldsymbol{\eta}$
$\boldsymbol{\eta}$ initial condition vector
$\boldsymbol{\eta}^0$ fixed point vector
τ time
τ_0 fundamental time period
ω_n normalizing frequency for impact pair
Ω fundamental excitation frequency
ξ viscous damping coefficient for Duffing oscillator
$\boldsymbol{\Psi}$ derivative vector of state vector w.r.t. parameter α
ζ non-dimensional viscous damping coefficient of impact pair

Subscripts

m mean
p alternating components
amp amplitude
i, j, k vector or matrix indices

Second order subscripts

i excitation harmonic index

Superscripts

1, 1* corrector step in the continuation scheme
k iteration step in Newton–Raphson scheme

Symbols

Δ correction or change in any parameter
$|\cdot|$ magnitude